Aerosol and Air Quality Research

ORIGINAL RESEARCH
https://doi.org/10.4209/aaqr.220114

Changes in Chemical Composition, Sources, and Health Risk of $PM_{2.5}$ with Sand Storm at a Small City in North China

Jihong Wei[1*], Ting Hou[1], Zhiyong Li[2,3*], Songtao Guo[2], Zhenxin Li[2]

[1] Department of Pediatrics, Affiliated Hospital of Hebei University, Baoding 071000, China
[2] Hebei Key Lab of Power Plant Flue Gas Multi-Pollutants Control, Department of Environmental Science and Engineering, North China Electric Power University, Baoding 071003, China
[3] MOE Key Laboratory of Resources and Environmental Systems Optimization, College of Environmental Science and Engineering, North China Electric Power University, Beijing 102206, China

ABSTRACT

Sand storm (SS) is highly concerned based on its adverse impacts on environment and health. A field observation was conducted in Dingxing County within the Beijing-Tianjin-Hebei region from 16 March to 9 April 2021 covering two SS episodes to evaluate the SS impacts on $PM_{2.5}$ components, health risks, and sources. From the non-SS period (NSSP) to the SS period (SSP), more increase was found in PM_{10} (114–300 μg m^{-3}) than $PM_{2.5}$ (61.5–75.2 μg m^{-3}), suggesting the obvious increment of coarse particles ($PM_{2.5-10}$) in the SSP. $PM_{2.5}$ reconstruction indicated that higher dust of 54.0 μg m^{-3} and trace element oxides (TEO) of 0.234 μg m^{-3} were found in the SSP, evidencing their immigration from the sand dust. In consequence, the elevated exposure risks via inhalation including carcinogenic and non-carcinogenic were found in the SSP. More attention should be paid to high non-carcinogenic risks of 2.49 for adults and children in the SSP. Again, the concentrations of organic carbon (OC) and secondary organic carbon (SOC) increased in the SSP, especially in the case of SOC. High usage of coal and biomass for heating purpose in Mongolia and Inner Mongolia might be an explanation. However, the mass contributions of nine water-soluble ions to $PM_{2.5}$ decreased from 54.0% to 33.5% due to their low contents in sand dust. Seven sources including construction dust (CD), biomass burning (BB), secondary inorganic aerosols (SIA), industrial emissions (IN), vehicle emissions (VE), coal combustion (CC), and soil dust (SD) were recognized by positive matrix factorization (PMF) model. SD was the biggest contributor in the SSP and accounted for 68.8% of the $PM_{2.5}$ mass. VE contributed highest to $PM_{2.5}$ in NSSP, indicating the effective emission control on industries and coal combustion.

Keywords: Sand storm, $PM_{2.5}$, Beijing-Tianjin-Hebei, Positive matrix factorization, Exposure risk

Received: March 6, 2022
Revised: April 17, 2022
Accepted: May 6, 2022

* **Corresponding Authors:**
Jihong Wei
15176257362@139.com
Zhiyong Li
lzy6566@126.com

Publisher:
Taiwan Association for Aerosol Research
ISSN: 1680-8584 print
ISSN: 2071-1409 online

1 INTRODUCTION

Serious air pollution has occurred frequently in present China, which has attracted the worldwide attention (Liu *et al.*, 2020; Jiang *et al.*, 2020; Li *et al.*, 2021; Yang *et al.*, 2022). Atmospheric aerosol is a complex mixture derived from anthropogenic and natural origins, affecting directly or indirectly the earth's atmosphere, ecosystems, and climate change (Hussein *et al.*, 2020; Cigánková *et al.*, 2021). A multitude of attention has been poured into $PM_{2.5}$, principally owning to the negative effects on human health (Zhu *et al.*, 2018; Barbara *et al*, 2020). Long-term exposure to high $PM_{2.5}$ can cause damages to respiratory and cardiovascular systems, and even premature death of humans (Karimi *et al.*, 2020).

The main anthropogenic sources of ambient $PM_{2.5}$ include industrial activities, energy production, construction, vehicle exhaust, and so on (Xu *et al.*, 2019; Si *et al.*, 2021). What's more,

sand storm (SS) mainly occurs at the arid deserts in northwestern China and Mongolia with low vegetation coverage and strong surface winds (Liang *et al.*, 2013; Alghamdi *et al.*, 2015; Hussein *et al.*, 2020). Sand dust can cause the large variations in chemical and surface properties of particles in SS path area, especially when it passes through the heavily polluted areas and mix with the local anthropogenic pollutants including heavy metals, carbonaceous aerosols, sulfates, and nitrates (Huang *et al.*, 2013; Alghamdi *et al.*, 2015). Former studies demonstrated that SS greatly elevated $PM_{2.5}$ and $PM_{2.5\text{-}10}$, and reduced visibility, and thus deteriorated air quality at a local, regional, and even global scale in certain duration of a few hours to a few days (Chen *et al.*, 2004; Lee *et al.*, 2006; Liang *et al.*, 2013; Alghamdi *et al.*, 2015). For instance, the sand dust from Mongolia can transport to eastern China, southeastern China, South Korea, and Japan, and subsequently brings about the adverse impacts on local air quality (Chen *et al.*, 2018; Jeong and Park, 2018). Meanwhile, the epidemiological studies have concluded that exposure to sand dust increased the daily mortality, exacerbate cardiovascular, and respiratory diseases (Wang *et al.*, 2016; Liu *et al.*, 2017; Karimi *et al.*, 2020).

Beijing-Tianjin-Hebei (BTH) region, the largest economic region in northern China, is often plagued by air pollution incidents and is vulnerable to SS events due to its geographic location. However, to our knowledge, the SS impacts on $PM_{2.5}$ levels, sources, and health risk still remained unclear in small cities within the North China Plain (NCP). In this study, an intensive field observation was carried out in a small county town named as Dingxing County, located 104 km south of Beijing city, during 16 March to 9 April 2021covering two SS episodes. The chemical components including organic carbon (OC), elemental carbon (EC), 9 water-soluble ions (WSIs) and 39 inorganic elements (IEs) were measured. This study was mainly aimed toward: 1) analyzing the variations of $PM_{2.5}$ and its components in both the NSSP and the SSP; 2) assessing the potential carcinogenic and non-carcinogenic risks posed by $PM_{2.5}$-bound heavy metals; and 3) identifying the impacts of SS on sources using a PMF model and the backward trajectory clustering analysis.

2 METHDOLOGY

2.1 Sampling Area Description

$PM_{2.5}$ samples were collected on the rooftop of a main building of Dingxing County Government (115.80°E; 39.25°N, approximately 25 m above ground). As shown in Fig. 1, Dingxing County is situated in the north of Hebei Province within the North China Plain (NCP). Furthermore, it is located in the central area of Beijing-Tianjin-Hebei (BTH) region, which is 89 kilometers south to Beijing City, 122 kilometers west to Tianjin City, and 54 kilometers north to Baoding City. The site is surrounded by residential buildings within a 3 km radius and thus can be categorized as a typical residential zone.

2.2 $PM_{2.5}$ Sampling

The sampling procedures were described in detail in Tao *et al.* (2014a) and Li *et al.* (2021). Two air samplers (TH-150C III, Wuhan Tianhong Ltd., China) set at 100 L min^{-1} were utilized to simultaneously collect $PM_{2.5}$. Ambient air PM_{10} has been online monitored on this site. The used filters included a 90 mm quartz fiber (QF) filter (Pall USA) and a 90 mm Teflon (PTEE) filter (Whatman UK). A total of 50 samples and 4 field blank samples were gathered from March 16 to April 9, 2021, and each sampling duration was 23 h (10:00 AM–9:00 AM of the next day). Prior to sampling, QF filters were baked at 450°C for 4 h and PTEE filters were also heated at 60°C. PTEE filters were stored in a room at a constant temperature (20°C) and relative humidity (50%) before and after sampling to obtain the $PM_{2.5}$ mass by subtracting pre-weight from post-weight. A series of field blank experiments were conducted to correct subsequent analysis deviation and ensure its accuracy.

2.3 Analysis of Elements

The detailed analysis procedures could be found in Li *et al.* (2021) and Yang *et al.* (2022), which were employed in this study. Each PTEE filter was cut into equal halves to analyze 30 elements (Li, Be, Na, P, K, Sc, V, Cr, Mn, Co, Ni, Cu, Zn, As, Rb, Y, Mo, Cd, Sn, Sb, Cs, La, Ce, Sm, W, Tl, Pb, Bi, Th, and U) using a ICP-MS (Agilent 7500a, USA) system, and 9 elements (Zr, Al, Sr, Mg, Ti, Ca, Fe, Ba, and Si) using an ICP-OES (Agilent 5100, USA) system. For ICP-MS, a half of filter was performed

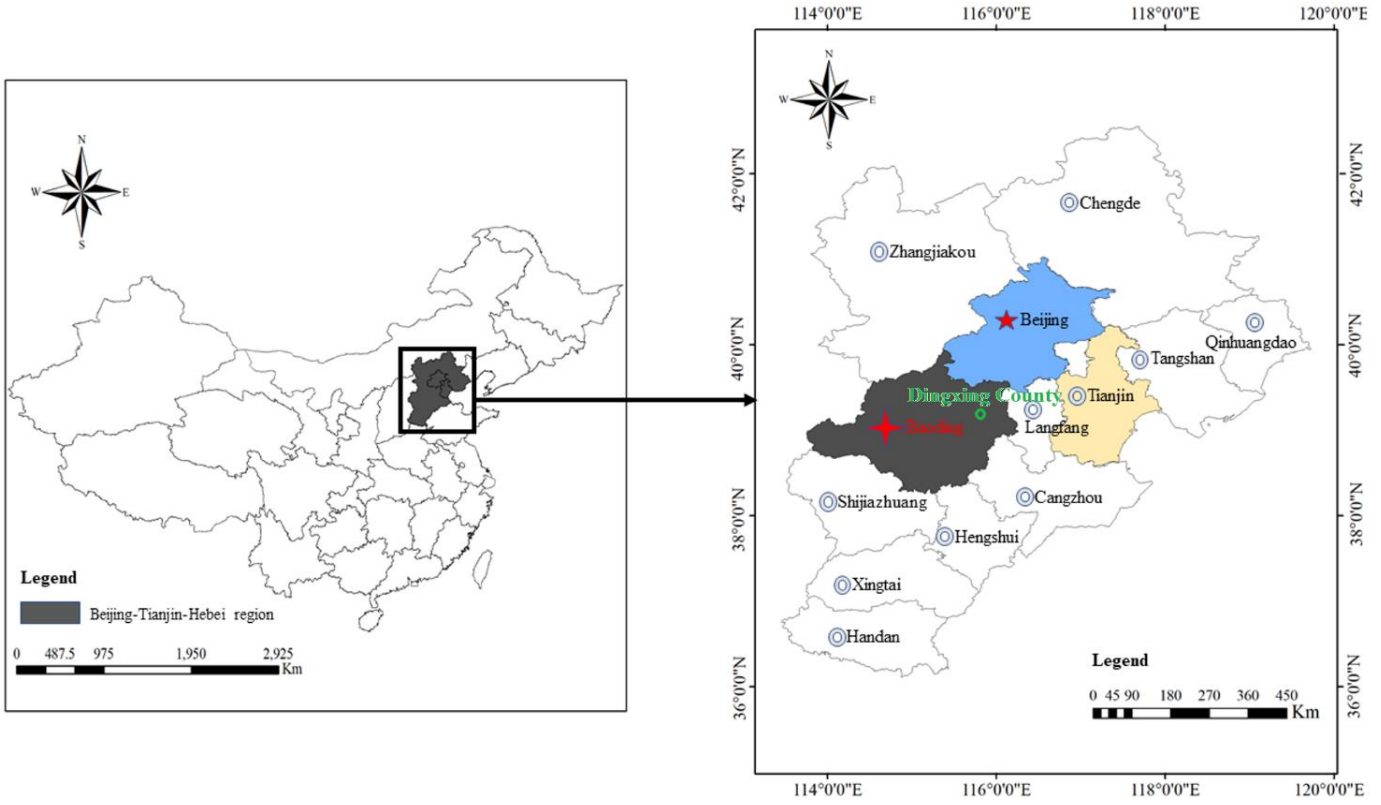

Fig. 1. Sampling location (green point) in Beijing-Tianjin-Hebei region.

with a mixed acid (aqua regia + HF) at 120°C for 2 h, and then dried at 130°C. Finally, it was heated again with HCl acid before analysis. Another half of filter for ICP-OES measurement was completely ashing at 550°C and digested with the absolute ethanol and NaOH, and then boiled with water. The recoveries for all the elements fell within ± 10% of the certified values. Calibration was carried out with multi-element standards (GBW07446-07457). Precision for most elements were better than 5% (n = 5). Additional information about the QA/QC and analytical procedures can be found in Tao *et al.* (2014a) and Li *et al.* (2021).

2.4 Analysis Water-Soluble Ions

A half of QF filter was cut into pieces and ultrasonically extracted for 20 minutes with 10 mL de-ionized water for at least three times. The extract was filtered using a microporous membrane with pore size as 0.22 μm (Whatman, Middlesex, UK), and then transferred into a clean centrifugal tube and sealed, and stored at 4°C before analysis. An ion chromatograph of ICS-1000 system (Thermo Scientific, USA) system and an ICP-OES system (Agilent 725, Agilent Co. USA) were employed to measure 4 anions (SO_4^{2-}, NO_3^-, Cl^-, and F^-) and 4 cations (K^+, Na^+, Ca^{2+}, and Mg^{2+}), respectively. The MDLs for ICP-1000 and ICP-OES fell within 0.004–0.012 and 0.002–0.023 μg mL^{-1}. An ultraviolet-visible spectrophotometer (UV-VIS, T6, Beijing General Instruments Co., Ltd.) was used to analyze NH_4^+ and the MDL was 0.003 μg mL^{-1}. The recoveries for all the 9 WSIs were within 100 ± 20%.

Field blank samples, replicate samples, and standard solutions obtained from the Research Center of China National Standard Reference Materials were analyzed for quality control and assurance.

2.5 Analysis of OC and EC

An area of 0.526 cm^2 punched from another half of QF filter was detected for OC and EC by a Sunset Model 5L carbon analyzer following the thermal/optical reflectance (TOR) protocol with the MDL was 0.2 μg cm^{-2} (Tao *et al.*, 2014a). The replicate analyses were performed within 5% error. The detailed information about analytical procedures and quality assurance/control have been illustrated in Tao *et al.* (2014a).

2.6 Health Risk Assessment

In this study, a risk assessment model recommended by U.S. EPA was obtained to evaluate the carcinogenic and non-carcinogenic risks posed by heavy metals in $PM_{2.5}$ (Hu *et al.*, 2012; Megido *et al.*, 2017; Si *et al.*, 2021). In this study, the health risks posed by three kinds of exposure ways including inhalation (inh), ingestion (ing), and dermal (derm) contact were calculated as the total risks (Si *et al.*, 2021). Detailed calculation method of exposure risk can be found in Hu *et al.* (2012) and Megido *et al.* (2017), and the corresponding parameters were listed in Table S1.

2.7 Positive Matrix Factorization Model Analysis

Positive Matrix Factorization (PMF) model is a widely used tool for the qualitative and quantitative analysis of pollutant sources (Yao *et al.*, 2016). More realistic factors can be obtained by PMF due to its non-negative constraints (Yao *et al.*, 2016; Lang *et al.*, 2018). PMF version 5.0 was utilized in this study, and the datasets of 39 elements, 9 water-soluble ions, organic carbon (OC), and elemental carbon (EC) were used as model inputs. Meanwhile, the abnormal values were eliminated to prevent error. The acquisition of missing values and associated uncertainties were demonstrated in detail in Yao *et al.* (2016) and Yang *et al.* (2022). A total of 20 runs were used for each chemical component. The lowest Q_{robust} value was 3090.12, and the ratio of Q_{robust}/Q_{true} was 0.91. More details on PMF were provided in previous studies (Yao *et al.*, 2016; Xu *et al.*, 2019).

2.8 Backward Trajectory Clustering

Backward trajectory clustering analysis was employed to evaluate the origins of air masses arrived at Dingxing County (Tao *et al.*, 2014a; Yao *et al.*, 2016). In this study, three-dimension 72-h backward trajectories of air masses arriving at Dingxing were calculated using a Hybrid Single Particle Lagrangian Integrated Trajectory (HYSPLIT-4) model. Finally, a total of six transport paths were obtained and their homogeneity within clusters was achieved by minimizing the angle distances.

3 RESULTS AND DISCUSSION

3.1 Concentrations of $PM_{2.5}$ and PM_{10}

The mean $PM_{2.5}$ was 64.8 μg m^{-3} in the entire sampling period (ESP), which attained the of 75 μg m^{-3} defined in the National Ambient Air Quality Standard Grade II (Fig. 2). As high as 80.0% of sampling days showed a daily $PM_{2.5}$ of lower than 75 μg m^{-3}, indicating the improvement of air quality caused by recent emission control policies (Zhai *et al.*, 2019). The $PM_{2.5}$ level (reported in μg m^{-3}) of 64.8 μg m^{-3} in this study was lower than 86.8 of Beijing in 2010–2016 (Zhu *et al.*, 2018), 91.7 of Shijiazhuang in 2016 (Lang *et al.*, 2018), 100.6 of Xinxiang in 2015 (Feng *et al.*, 2018), which concurred with the present decreasing trend of $PM_{2.5}$ on a national scale (Li *et al.*, 2021; Si *et al.*, 2021). On average, $PM_{2.5}$ elevated from 61.5 μg m^{-3} in the NSSP to 75.2 μg m^{-3} in the SSP (16^{th}–17^{th} March, and 28^{th}–31^{st} March). More increase was found in PM_{10} and noticeably increased from 114 to 300 μg m^{-3}, which reflected relative high coarse particles were contained in sand dust (Alghamdi *et al.*, 2015). Furthermore, the mass ratios of $PM_{2.5}/PM_{10}$ decreased from 0.549 in the NSSP to 0.248 in the SSP. The lower $PM_{2.5}/PM_{10}$ ratios in the SSP indicated Dingxing County was susceptible to the serious pollutions of $PM_{2.5\text{-}10}$ due to the sand storm episode (Alghamdi *et al.*, 2015).

3.2 Inorganic Elements

Fig. 3 presented the average concentrations of 39 elements in $PM_{2.5}$, and their changes between the NSSP and the SSP. The fugitive dust and trace element oxides (TEO) were reconstructed according to the documented method in Su *et al.* (2017) and Zhang *et al.* (2013a). The expressions were shown as follows: [Dust] = 2.20 × [Al] + 2.49 × [Si] + 1.63 × [Ca] + 1.42 × [Fe] + 1.94 × [Ti], and TEO = 1.3 × [0.5 × (Sr + Ba + Mn + Co + Rb + Ni + V) + 1.0 × (Cu + Zn + Mo + Cd + Sn + Sb + Tl + Pb + As + Cs + Se + Ge + Ga)]. Due to the data lack of Se, Ge, and Ga, the TEO was underestimated slightly. The mass contributions of total eight crustal elements Si, Al, Fe, Ca, K, Mg, Na, and Ti to $PM_{2.5}$ enhanced from 10.9% in the NSSP to 36.0% in the SSP. Accordingly, the reconstructed dust concentrations increased from 11.7 to 54.0 μg m^{-3} with the mass share in $PM_{2.5}$ elevated from 19.0% to 71.8% (Fig. 2).

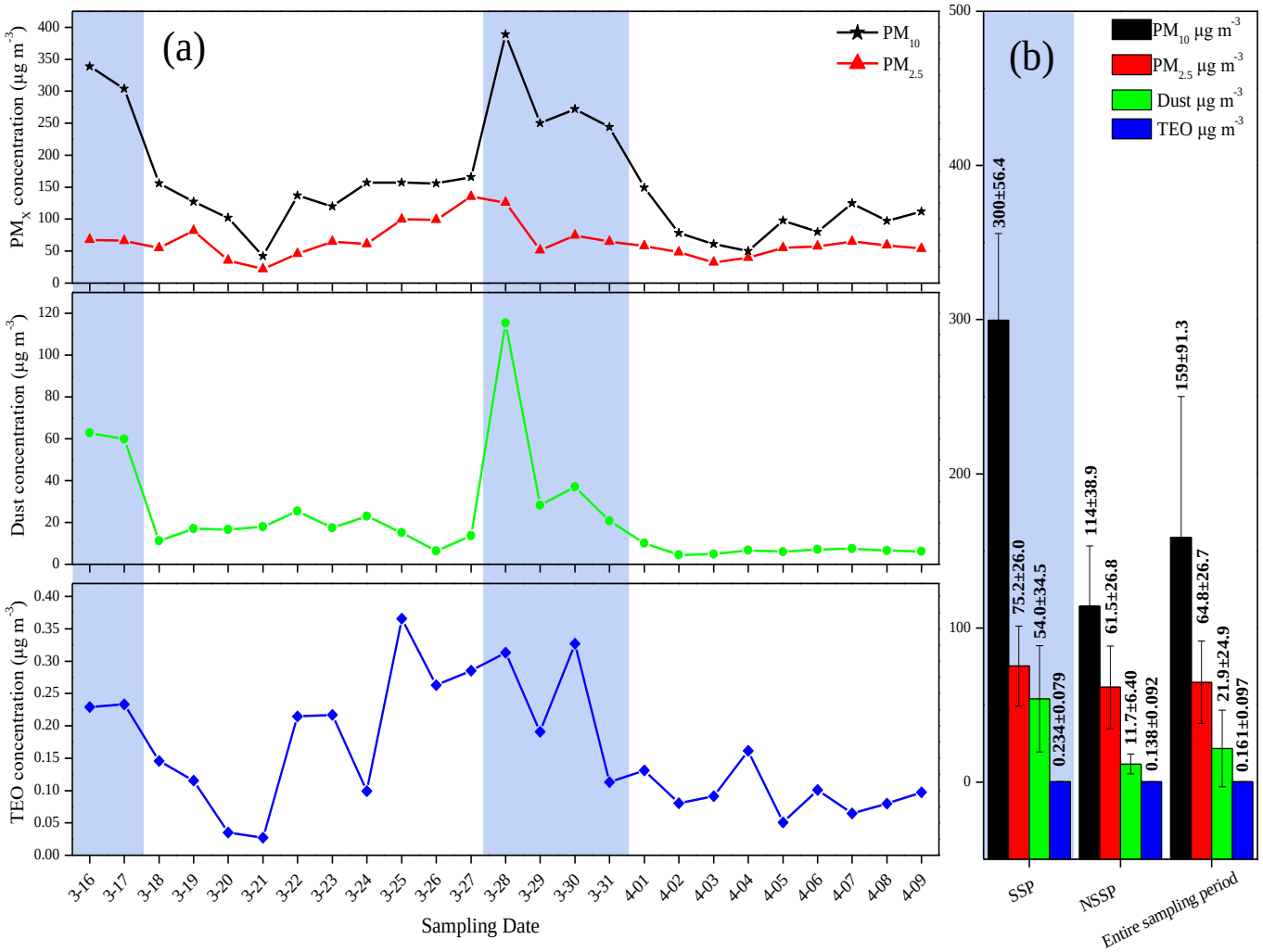

Fig. 2. Concentrations of $PM_{2.5}$, PM_{10}, and reconstructed dust and TEO for (a) each sampling day, and (b) the NSSP, the SSP, and the entire sampling period.

High levels of all the elements except for Ni, Cu, and Sn were found in the SSP. The decreased Ni and Cu might be caused by emission reductions from vehicles, and Sn should be attributed to the emission control on industries (Xu *et al.*, 2019; Si *et al.*, 2021). Meanwhile, TEO concentrations elevated from 0.138 μg m^{-3} in the NSSP to 0.234 μg m^{-3} in the SSP. Large amounts of concerned heavy metals As, Mn, Cr, Co, V, Sc, Tl, Pb, Cd, Zn, Sb, and Rb from industries in Inner Mongolia caused their increases in Dingxing by 312%, 131%, 333%, 506%, 740%, 28.0%, 20.1%, 93.6%, 21.8%, 40.9%, 472%, respectively in the SSP (Xu *et al.*, 2019). A large number of industries including coal-combustion power plants, iron-steel production, and non-ferrous metal processing clustered in Inner Mongolia further proved above suggestion (Si *et al.*, 2021).

3.3 Water-Soluble Ions

Water-soluble ions (WSIs) were formed by secondary reactions between the primary emitted pollutants and played a decisive role in the process of aerosol hygroscopicity, which could aggravate the visibility impairment (He *et al.*, 2017). WSIs generally contributed to 20–45% or even > 70% of the $PM_{2.5}$ mass (He *et al.*, 2017). In this study, Σ_9WSIs decreased from 36.8 μg m^{-3} in the NSSP to 23.4 μg m^{-3} in the SSP, and the contributions reduced accordingly from 54.0% to 33.6%. The air pollutants contained in sand dust originated mainly from primary emissions would be the explanation. SO_4^{2-}, NO_3^-, and NH_4^+ dominated in WSIs and constituted 73.2 ± 19.0% of the $\sum_9$WSIs, which was mainly attributed to the reactions among local gaseous pollutants. The correlation coefficients between SO_4^{2-}, NO_3^-, NH_4^+, and $PM_{2.5}$ were higher in the NSSP than those in the SSP

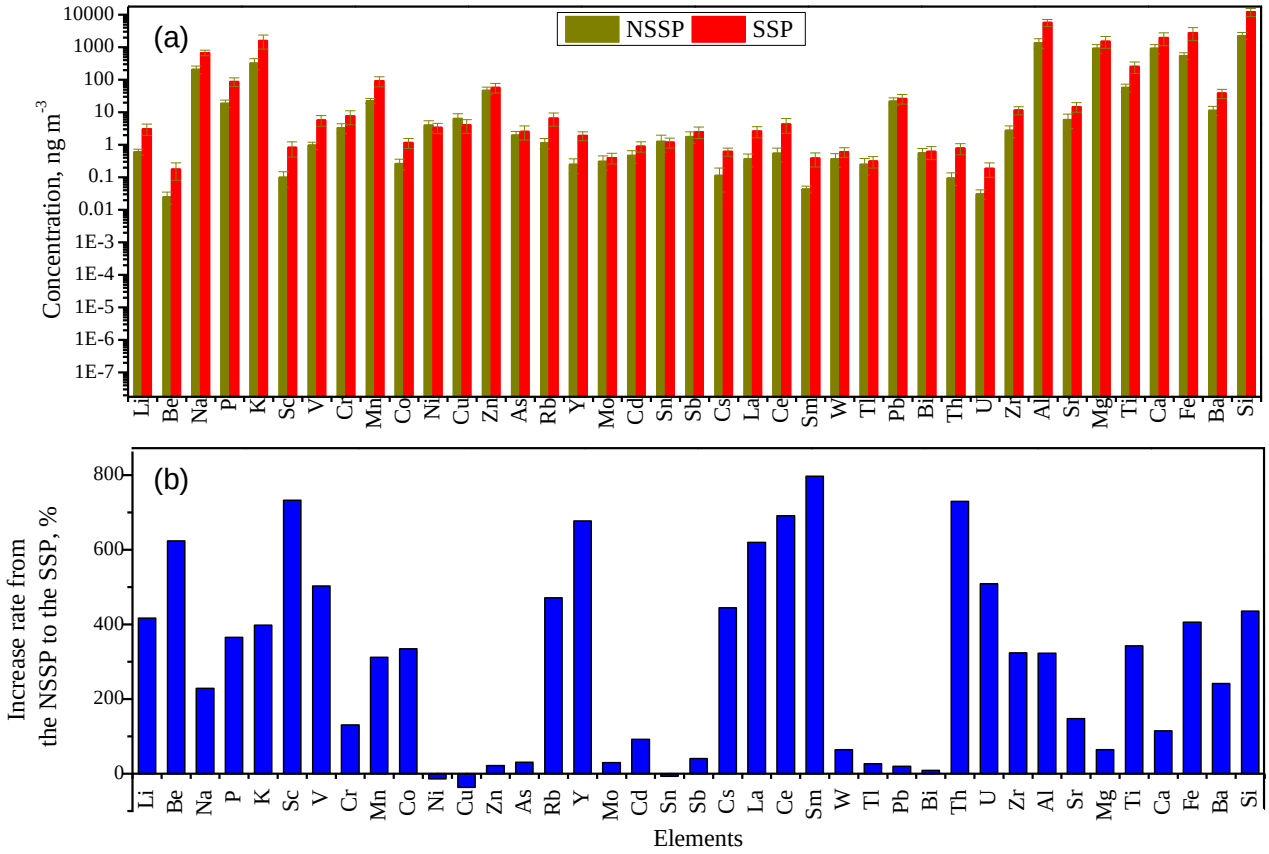

Fig. 3. (a) Concentrations of the thirty-nine elements, and (b) their increase rates from the NSSP to the SSP.

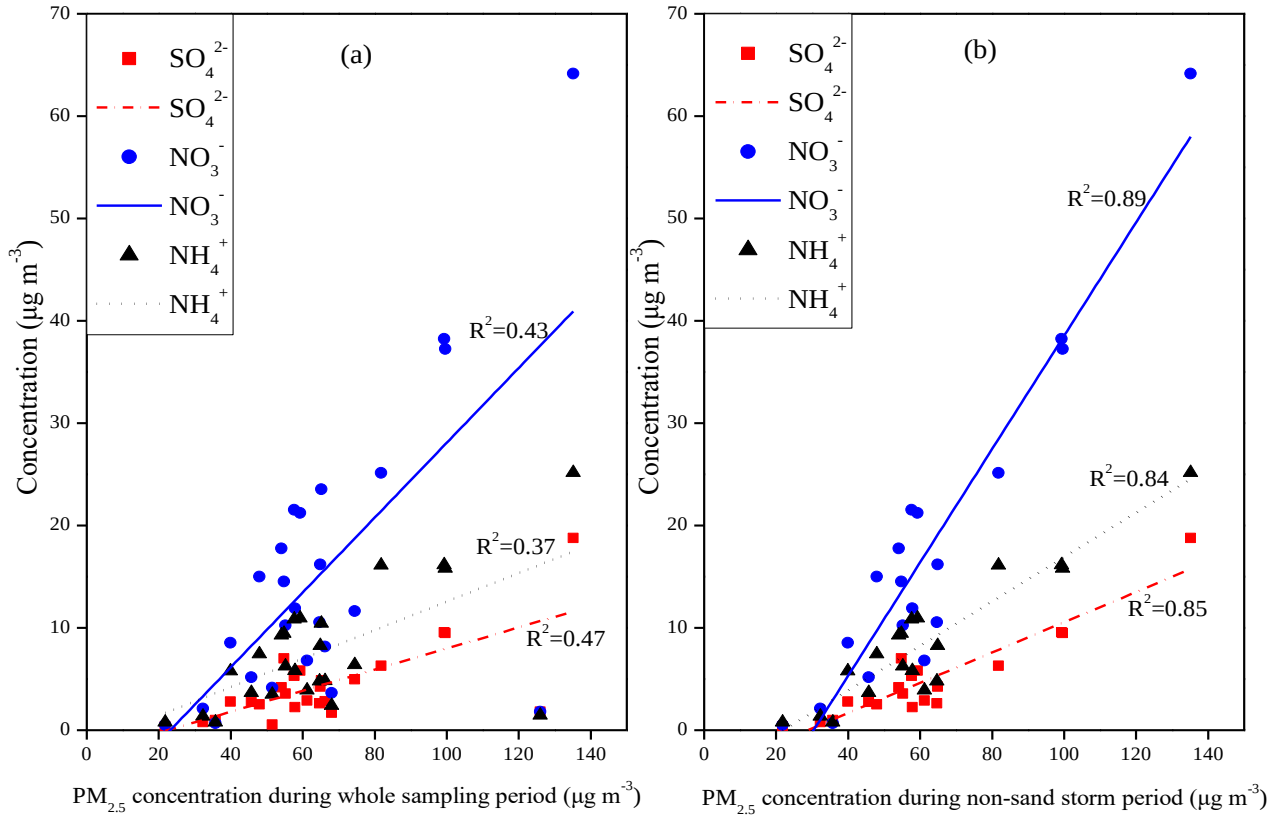

Fig. 4. Correlations between SO_4^{2-}, NO_3^-, NH_4^+, and $PM_{2.5}$ in (a) the entire sampling period, and (b) the sand storm period.

(Fig. 4). Weak correlations in the SSP were ascribed to the increase in $PM_{2.5}$ and decrease in WSIs. The NO_3^-/SO_4^{2-} ratio was a widely used indicator to evaluate the relative importance of stationary and mobile sources (He *et al.*, 2017). Mean NO_3^-/SO_4^{2-} ratios were up to 3.49 in SSP and 3.33 in NSSP, indicating the impacts of natural gas burning for heating when emission reductions in vehicles were taken into account (Meng *et al.*, 2020; Pozzer *et al.*, 2020). The heating period was extended to 31 March due to the COVID-19 event, and two SS episodes were all within the heating period. Therefore, large NG consumptions in heating period resulted in higher NO_3^-/SO_4^{2-} ratio in the SSP. Meanwhile, this ratio in 2020 was much higher than 0.95 for Shijiazhuang in 2016 (Lang *et al.*, 2018) and 1.90 for Tianjin in 2018–2019 (Tang *et al.*, 2021), which was attributed to higher and higher replacement rate of coal by NG (Meng *et al.*, 2020).

To quantify the atmospheric transformation of SO_2 to SO_4^{2-} and NO_2 to NO_3^-, the sulfur oxidation ratio (SOR) and nitrogen oxidation ratio (NOR) were calculated as following equations:

$$SOR = nSO_4^{2-}/(nSO_4^{2-} + nSO_2) \quad (1)$$

$$NOR = nNO_3^-/(nNO_3^- + nNO_2) \quad (2)$$

Where n refers to the molar concentration. SORs and NORs in both the SSP and the NSSP were all higher than 0.10, evidencing the existence of photochemical oxidation of SO_2 to SO_4^{2-} and NO_2 to NO_3^- (He *et al.*, 2017). On average, higher SOR and NOR of 0.233 and 0.221 were found in the NSSP than the corresponding 0.154 and 0.112 in the SSP, suggesting the weakening effect on oxidation process of gas precursors due to low relative humidity in the SSP.

3.4 Organic Carbon and Elemental Carbon

Higher mean organic carbon (OC) concentration of 8.48 μg m^{-3} was found in the SSP compared with 6.23 μg m^{-3} in the NSSP. As the SS source region, Inner Mongolia possesses abundant coal resource with low coal to gas penetration rate in heating season, which result in high emissions of OC (Chen *et al.*, 2018). In consequence, high OC-containing SS flushed out of the Inner Mongolia and moved into Dingxing County, and elevated the local OC concentration. Elemental carbon (EC) is usually used as a tracer of primary OC (POC) due to its incomplete combustion of carbonaceous fuel, inertia in the atmosphere, and co-emission with OC (Tao *et al.*, 2014b). Secondary organic carbon (SOC) can be formed through atmospheric photo chemical reactions. The OC/EC ratio has been considered as an indicator of the relative contribution of primary and secondary organic aerosols (SOA) (Tao *et al.*, 2014b). It is generally believed that SOC may be formed if the OC/EC ratio overtops 2.0–2.2 though the sampling duration and analysis methods may lead to different OC/EC ratios (Zhang *et al.*, 2013b). Higher OC/EC ratio of 4.84 in the SSP was found compared with 2.76 in NSSP, indicating stronger formation of SOC in the SSP (Fig. 5). Meanwhile, SOC was calculated to estimate its contribution to OC by the following equation: SOC = OC – POC = OC – EC × $(OC/EC)_{min}$, where OC (μg m^{-3}) is the concentration of OC, EC (μg m^{-3}) is the concentration of EC, and $(OC/EC)_{min}$ is the minimum OC/EC ratio during the entire sampling period. The average SOC concentrations were 4.62 and 1.33 μg m^{-3} in the SSP and the NSSP, which accounted for 54.5% and 21.3% of the OC mass, respectively.

3.5 Health Risks Posed by Heavy Metals

The total CRs by three exposure pathways to As, Cd, Co, Cr(VI), Ni, and Pb for children and adults were 1.72×10^{-4} and 1.17×10^{-4} in the SSP, and 2.04×10^{-4} and 1.15×10^{-4} in the NSSP, and all of them exceeded the acceptable level (1×10^{-4}) (Fig. 6) (Megido *et al.*, 2017). Differences in CRs for adults and children between the NSSP and the SSP were mainly attributed to the variations in Ni and Cr (Table S2). The CRs followed the order of $CR_{ing} > CR_{derm} > CR_{inh}$ in both the NSSP and the SSP for children, and in the NSSP for adults, while they were CR_{ing} (4.94×10^{-5}) > CR_{inh} (3.87×10^{-4}) > CR_{derm} (2.87×10^{-4}) for adults in the SSP. The fluctuations in Ni and Cr, and the differences in parameters between children and adults would be the explanation.

For CRs posed by three pathways, Ni was the biggest contributor to children, followed by As and Cr (Table S2). Ni possessed the CRs up to 1.36×10^{-4} for children in the NSSP, then decreased to 8.00×10^{-5} in the SSP due to the effective emission-reductions from traffic and oil-burning related

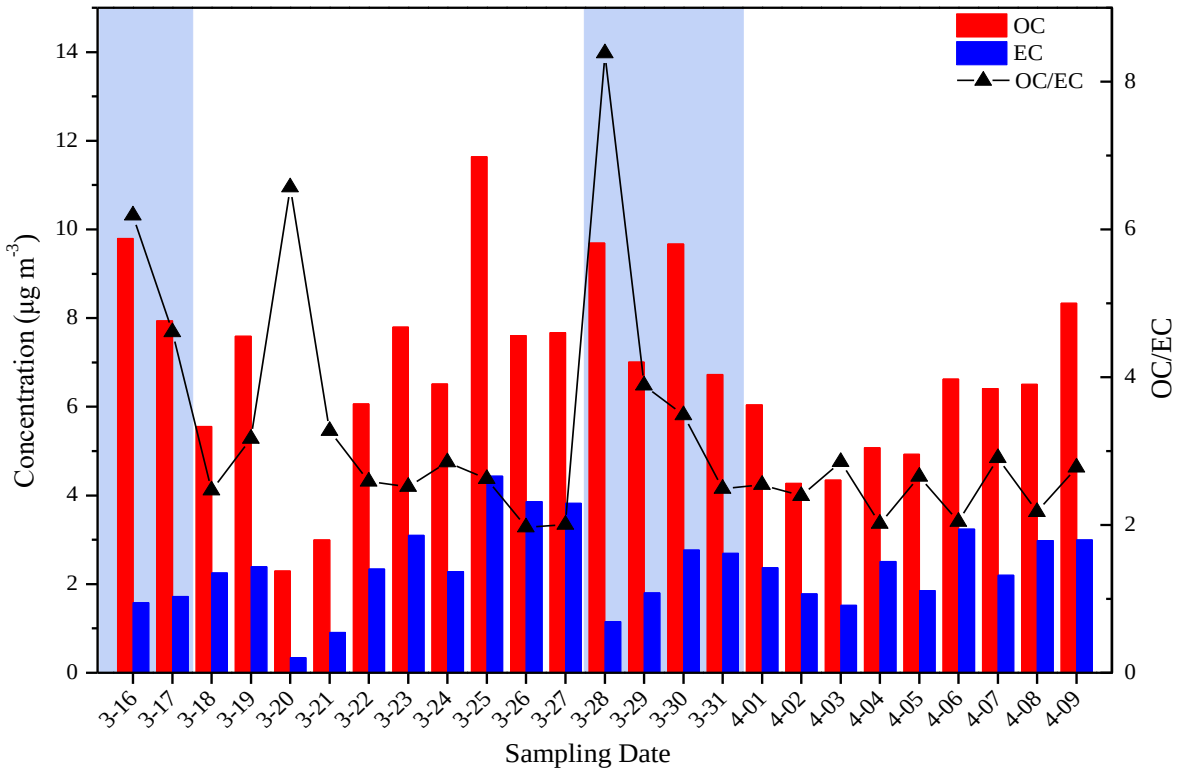

Fig. 5. Time series of OC, EC, and ratios of OC/EC.

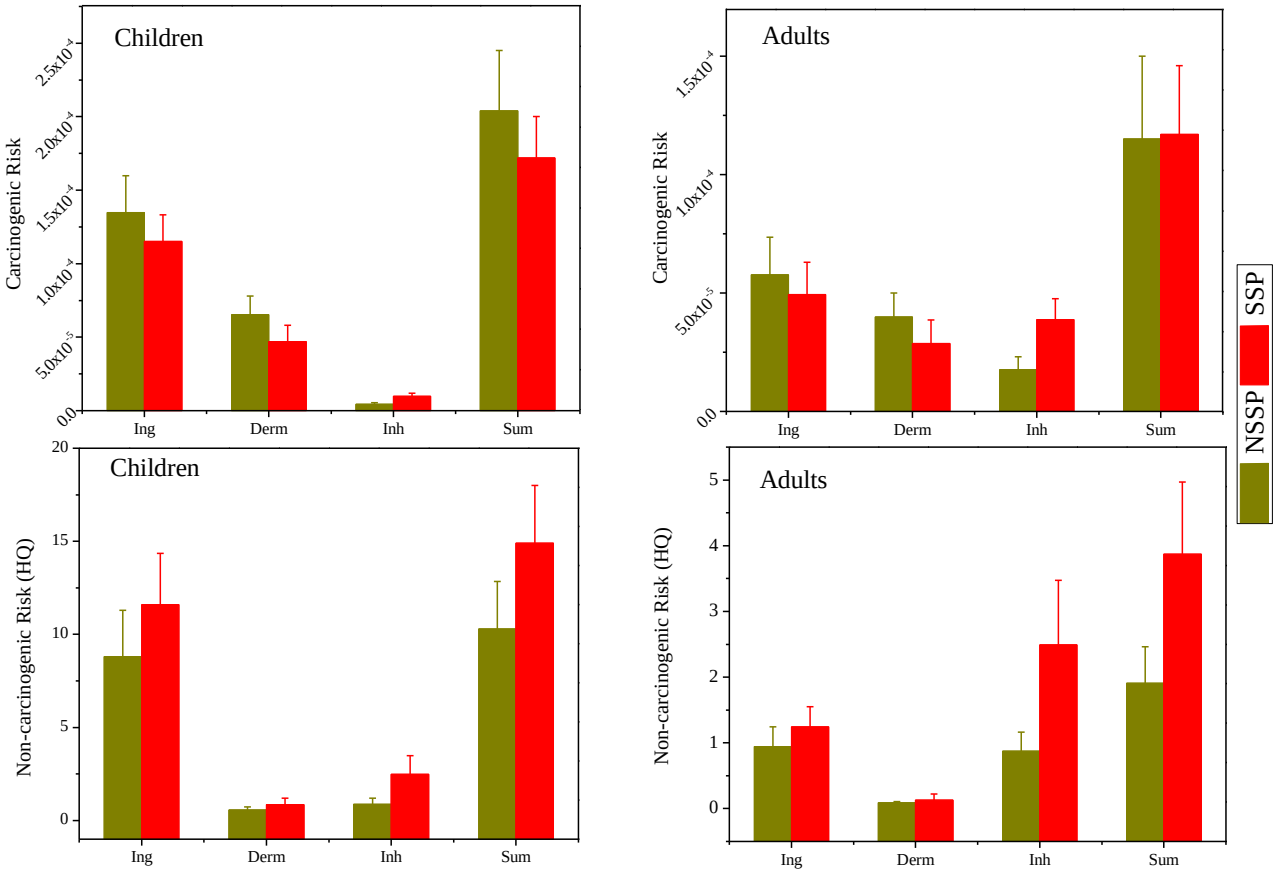

Fig. 6. Carcinogenic and non-carcinogenic risk posed by $PM_{2.5}$-bounded elements via inhalation, dermal contact, and ingestion exposure.

enterprises. CRs for children caused by As enhanced from 5.51×10^{-5} in the NSSP to 6.61×10^{-5} in the SSP (Table S2).

In regard to the inhalation, CRs increased from 4.40×10^{-6} in the NSSP to 9.69×10^{-6} in the SSP for children, and from 1.76×10^{-5} to 3.87×10^{-5} for adults. This suggestion was in agreement with higher As, Co, and Cr in the SSP. Furthermore, CRs in the NSSP for children caused by inhalation in this study were lower than 1.25×10^{-5} for Shijiazhuang and 1.18×10^{-5} for Baoding in 2016 (Si *et al.*, 2021), and 7.70×10^{-6} of Shijiazhuang and 7.60×10^{-6} of Baoding in 2017 (Si *et al.*, 2021), which concurred with the decreasing trends of $PM_{2.5}$ and heavy metals in present China due to implementation of the "Clean Air Action" since 2013 (Zhai *et al.*, 2019). However, higher CRs for children in Dingxing County were found compared than Baoding and Shijiazhuang in 2017 under the SS effects. Coal-banning area was established in BTH region, and adjacent Shandong and Henan Province, therefore, the coal usage for heating in Inner Mongolia caused the increase of As, Co, and Cr in Dingxing county (Zhai *et al.*, 2019).

A total of 16 heavy metals Cu, Zn, As, Mo, Cd, Sn, Sb, Co, V, Cr, Mn, Ni, Pb, Tl, Fe, and Ba were used to evaluated the non-carcinogenic risks (NCRs). NCRs expressed as HQs posed by three exposure pathways increased from 10.3 in the NSSP to 14.9 in the SSP for children, and from 1.91 to 3.87 for adults, respectively (Fig. 6). For children, Tl had the highest HQ of 4.78 in the NSSP and 5.79 in the SSP (Tables S3 and S4), followed by Mn, As, Pb, and Sb. For adults, they were Mn > Tl > As > Co > Ni. The increased HQs for children and adults in the SSP might be related to the metal inputs from Inner Mongolia with high coal consumptions for heating (Xu *et al.*, 2019; Si *et al.*, 2021). For NCRs via inhalation for Baoding in 2016 and 2017, the comparable value for children was found in Dingxing in the NSSP (Si *et al.*, 2021). However, much higher value of 2.49 for both children and adults was found in Dingxing County compared than Baoding in 2016 (0.90) and 2017 (0.72) (Si *et al.*, 2021).

Based on the results above, potential CRs and NCRs posed by heavy metals in $PM_{2.5}$ for children and adults should not be neglected. More attention should be poured into the health risks in the SSP.

3.6 Source Apportionment by PMF Model

The source profiles were listed in Fig. S3, and a total of seven sources were obtained by PMF analysis. Factor 1 was represented by high loadings of Ca^{2+} and Mg^{2+}, which was attributed to the construction dust (CD) (Tao *et al.*, 2014a; He *et al.*, 2017). Factor 2 was composed by high Cl^- and K^+, and specific levels of NH_4^+, which was identified as biomass burning (BB) (Tao *et al.*, 2014a; Yao *et al.*, 2016; Yang *et al.*, 2022). Factor 3 was characterized by high levels of SO_4^{2-}, NO_3^-, and NH_4^+, indicating the secondary inorganic aerosols (SIA) (Zhang *et al.*, 2013b). Factor 4 comprised a high level of Bi, and specific contents of Pb, Zn, and Sn, which was attributed to industrial emissions (IN). Bi was found in metallurgical additives and alloy manufacturing (Sternbeck *et al.*, 2002). Pb, Zn, and Sn were also used in alloy manufacturing (Si *et al.*, 2021). Factor 5 was represented by a high load of Cu, Zn, and Pb, which was suggested to be vehicle emissions (VE) (Xu *et al.*, 2019). *Cu and Zn have been demonstrated to be good markers of VE*, and Pb was also found in vehicle exhaust (Xu *et al.*, 2019). Factor 6 was identified as coal combustion (CC) with high loadings of As and Cl^-, and certain levels of Pb and Tl (Tao *et al.*, 2014a; Wang *et al.*, 2015). Factor 7 was represented by high levels of crustal elements including Al, Fe, Si, Ti, Ba, Mg, and Sr, which was attributed to the soil dust (SD) (Tao *et al.*, 2014a; Xu *et al.*, 2019).

Fig. 7 showed the source contributions of seven emission sources during the ESP, SSP, and NSSP. SD was the biggest mass contributor (37.6%) of $PM_{2.5}$ during the ESP, followed by VE (20.4%), SIA (14.0%), CC (9.52%), CD (7.09%), BB (5.77%), and IN (5.65%), respectively, indicating the strong impact of SS episode. SD shares prevailed in SSP and its contribution was as high as 68.8%, while VE was the biggest contributor (27.5%) in NSSP due to the influence of intensive traffic in adjacent National Highway 107. Attributing to the COVID-19 incident, the heating period in Dingxing County extended from 15 March to 31 March, thus the CC contribution was comparable between NSSP and ESP. CC share (9.65%) in NSSP was significantly lower than 18.3% in Shijiazhuang, 22.6% in Baoding, 17.1% in Cangzhou in 2015–2016, and 13.6% in Luoyang City in 2019, which was attributed to the implementation of "Coal Prohibition" in 2017, which indicated the "Coal Prohibition" had been continuously strengthened (Si *et al.*, 2021). IN accounted for 9.48% in NSSP and lower than 20.5% in Shijiazhuang City, 13.5% in Baoding City, 11.7% in Cangzhou City in 2015–2016 (Xu *et al.*, 2019),

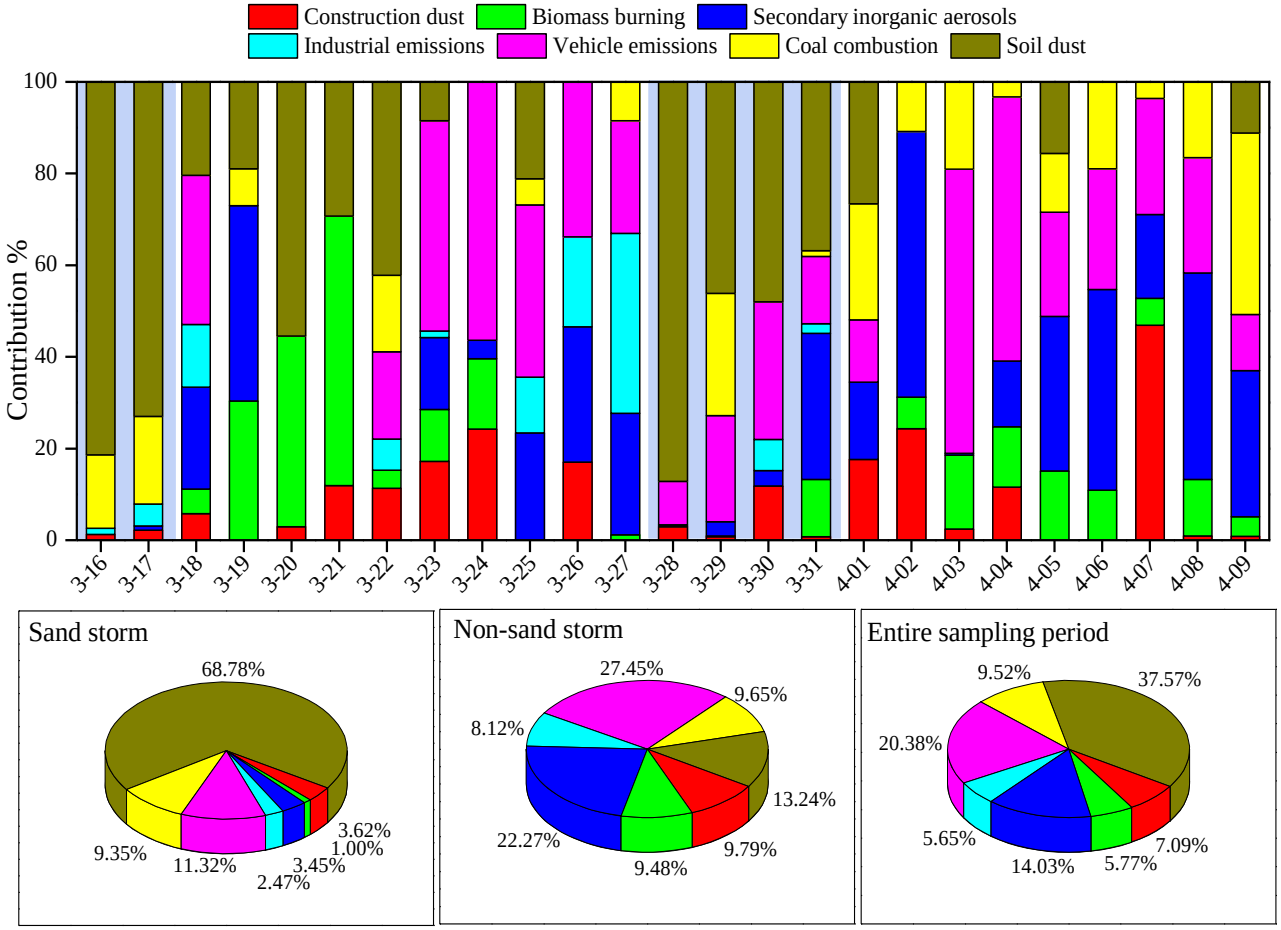

Fig. 7. Time series of source contributions to $PM_{2.5}$, and average source contributions in the NSSP, the SSP, and the entire sampling period.

which was attributed to better control enforcement in industrial emissions recently or lower industrial scale in small cities (Zhai *et al.*, 2019). BB share of 9.48% in the NSSP was higher than 5.3% in Tianjin City in 2014–2015 (Huang *et al.*, 2017), and 4.5% and 4.1% in Beijing in 2014–2015 and 2017–2018 (Huang *et al.*, 2017; Huang *et al.*, 2021), indicating the biomass-burning prohibition should be strengthened.

3.7 Backward Trajectory Analysis

Fig. S4 showed the backward trajectories of air masses arrived at Dingxing County. The main transportation routes could be divided into six categories. 20.2% of them originated from the northeast Bohai Sea area, 17.9% from Mongolia, 21.4% from the southern boundary of Hebei Province, 23.8% from Cangzhou City, 8.33% from Jiangsu Province and through Shandong Province, 8.33% from Inner Mongolia and through northern Hebei and Beijing.

4 CONCLUSIONS

A systematic $PM_{2.5}$ sampling campaign was conducted from 16th March to 9th April in 2021 covering two sand-storm (SS) episodes at an urban area within the central area of Beijing-Tianjin-Hebei (BTH) region, which aimed toward the impact evaluation of sand-storm on $PM_{2.5}$ sources, risk, and components.

1) $PM_{2.5}$ and PM_{10} increased by 22.3% and 163% in the sand-storm period (SSP) compared with those in the non-SS period (NSSP). Lower $PM_{2.5}/PM_{10}$ ratios in the SSP indicated that the sampling site was susceptible to coarse particles ($PM_{2.5-10}$).

2) The mass ratios of reconstructed dust in $PM_{2.5}$ increased from 19.0% in the NSSP to 71.8% in the SSP. High trace element oxides (TEO) were found in the SSP, which was attributed to the pollutant inputs from coal-related enterprises in Inner Mongolia. The carcinogenic risks (CRs) by inhalation increased from 4.40×10^{-6} in the NSSP to the 9.69×10^{-6} in the SSP for children, and from 1.76×10^{-5} to 3.87×10^{-5} for adults. Again, non-CRs by inhalation increased from 0.874 to 2.49 for both children and adults.

4) PMF indicated that soil dust (SD) was the biggest contributor in the entire sampling period (ESP) and constituted 68.8% of the $PM_{2.5}$ mass in the SSP. Vehicle emission contributed most of 27.5% to the $PM_{2.5}$ in the NSSP, indicating it should be further managed. Coal combustion occupied a share of 9.52% in $PM_{2.5}$ mass during the entire sampling period, which indicated that coal was still an important fuel for cooking/heating or industrial production.

ACKOWNLEGEMENTS

This study was supported by the Science and Technology Projects of Baoding (2141ZF321), the Beijing Natural Science Foundation (8212034), the Natura Science Foundation of Hebei Province (B2020502007), the Fundamental Research Funds for the Central Universities (2020MS125), and the "Three Three Three Talent Project" of Hebei Province (A202001055).

SUPPLEMENTARY MATERIAL

Supplementary material for this article can be found in the online version at https://doi.org/10.4209/aaqr.220114

REFERENCES

Alghamdi, M.A., Almazroui, M., Shamy, M., Redal, M.A., Alkhalaf, A.K., Hussein, M.A., Khoder, M.I. (2015). Characterization and elemental composition of atmospheric aerosol loads during springtime dust storm in western Saudi Arabia. Aerosol Air Qual. Res. 15, 440–453. https://doi.org/10.4209/aaqr.2014.06.0110

Barbara, B., Zioła, N., Mathews, B., Klejnowski, K., Słaby, K. (2020). The role of $PM_{2.5}$ chemical composition and meteorology during high pollution periods at a suburban background station in southern Poland. Aerosol Air Qual. Res. 20, 2433–2447. https://doi.org/10.4209/aaqr.2020.01.0013

Chen, Q.C., Wang, M.M., Sun, H.Y., Wang, X., Wang, Y.Q., Li, Y.G., Zhang, L.X., Mu, Z. (2018). Enhanced health risks from exposure to environmentally persistent free radicals and the oxidative stress of $PM_{2.5}$ from Asian dust storms in Erenhot, Zhangbei and Jinan, China. Environ. Int. 121, 260–268. https://doi.org/10.1016/j.envint.2018.09.012

Chen, S.J., Hsieh, L.T., Kao, M.J., Lin, W.Y., Huang, K.L., Lin, C.C. (2004). Characteristics of particles sampled in southern Taiwan during the Asian dust storm periods in 2000 and 2001. Atmos. Environ. 38, 5925–5934. https://doi.org/10.1016/j.atmosenv.2004.07.006

Cigánková, H., Mikuška, P., Hegrová, J., Pokorná, P., Schwarz, J., Krajčovič, J. (2021). Seasonal variation and sources of elements in urban submicron and fine aerosol in Brno, Czech Republic. Aerosol Air Qual. Res. 21, 200556. https://doi.org/10.4209/aaqr.2020.09.0556

Feng, J.L., Yu, H., Mi, K., Su, X.F., Li, Y., Li, Q.L., Sun, J.H. (2018). One year study of $PM_{2.5}$ in Xinxiang city, North China: Seasonal characteristics, climate impact and source. Ecotox. Environ. Safe. 154, 75–83. https://doi.org/10.1016/j.ecoenv.2018.01.048

He, Q.S., Yan, Y.L., Guo, L.L., Zhang, Y.L., Zhang, G.X., Wang, X.M. (2017). Characterization and source analysis of water-soluble inorganic ionic species in $PM_{2.5}$ in Taiyuan city, China. Atmos. Res. 184, 48–55. https://doi.org/10.1016/j.atmosres.2016.10.008

Hu, X., Zhang, Y., Ding, Z.H., Wang, T.J., Lian, H.Z., Sun, Y.Y., Wu, J.C. (2012). Bioaccessibility and health risk of arsenic and heavy metals (Cd, Co, Cr, Cu, Ni, Pb, Zn and Mn) in TSP and $PM_{2.5}$ in Nanjing, China. Atmos. Environ. 57, 146–152. https://doi.org/10.1016/j.atmosenv.2012.04.056

Huang, H., Song, W., Liu, X.Y. (2021). Significant contributions of combustion-related NH_3 and

non-fossil fuel NO_x to elevation of nitrogen deposition in southwestern China over the past five decades. Global Change Biol. 27, 4392–4402. https://doi.org/10.1111/gcb.15736

Huang, X.J., Liu, Z.R., Hu, B., Wen, T.X., Tang, G.Q., Zhang, J.K., Wu, F.K., Ji, D.S., Wang, L.L., Wang, Y.S. (2017). Chemical characterization and source identification of $PM_{2.5}$ at multiple sites in the Beijing-Tianjin-Hebei region, China. Atmos. Chem. Phys. 17, 12941–12962. https://doi.org/10.5194/acp-17-12941-2017

Huang, X.X., Wang, T.J., Jiang, F., Liao, J.B., Cai, Y.F., Yin, C.Q., Zhu, J.L., H, Y. (2013). Studies on a severe dust storm in East Asia and its impact on the air quality of Nanjing, China. Aerosol Air Qual. Res. 13, 179–193. https://doi.org/10.4209/aaqr.2012.05.0108

Hussein, T., Li, X.Y., Al-Dulaimi, Q., Daour, S., Atashi, N., Viana, M., Alastuey, A., Sogacheva, L., Arar, S., Al-Hunaiti, A., Petaja, T. (2020). Particulate matter concentrations in a middle eastern city - An insight to sand and dust storm episodes. Aerosol Air Qual. Res. 20, 2780–2792. https://doi.org/10.4209/aaqr.2020.05.0195

Jeong, J.I., Park, R.J. (2018). Efficacy of dust aerosol forecasts for East Asia using the adjoint of GEOS-Chem with ground-based observations. Environ. Pollut. 234, 885–893. https://doi.org/10.1016/j.envpol.2017.12.025

Jiang, H., Xiao, H., Song, H., Liu, J., Wang, T., Cheng, H., Wang, Z. (2020). A long-lasting winter haze episode in Xiangyang, Central China: Pollution characteristics, chemical composition, and health risk assessment. Aerosol Air Qual. Res. 20, 2859–2873. https://doi.org/10.4209/aaqr.2020.02.0068

Karimi, S.M., Pouran, H., Majbouri, M., Moradi-Lakeh, M., Hakimian, H. (2020). Saharan sand and dust storms and neonatal mortality: Evidence from Burkina Faso. Sci. Total Environ. 729, 139053. https://doi.org/10.1016/j.scitotenv.2020.139053

Lang, J.L., Li, S.Y., Cheng, S.Y., Zhou, Y., Chen, D.S., Zhang, Y.Y., Zhang, H.Y., Wang, H.Y. (2018). Chemical characteristics and sources of submicron particles in a city with heavy pollution in China. Atmosphere 9, 388–407. https://doi.org/10.3390/atmos9100388

Lee, C.T., Chuang, M.T., Chan, C.C., Cheng, T.J., Huang, S.L. (2006). Aerosol characteristics from the Taiwan aerosol supersite in the Asian yellow-dust periods of 2002. Atmos. Environ. 40, 3409–3418. https://doi.org/10.1016/j.atmosenv.2005.11.068

Li, Z.Y., Yue, Z.Y., Yang, D.Y., Wang, L., Wang, X., Li, Z.X., Wang, Y.T., Chen, L., Guo, S.T., Yao, J.S., Lou, X., Xu, X.L., Wei, J.Y. (2021). Levels, chemical compositions, and sources of $PM_{2.5}$ of rural and urban area under the impact of wheat harvest. Aerosol Air Qual. Res. 21, 210026. https://doi.org/10.4209/aaqr.210026

Liang, C.S., Yu, T.Y., Chang, Y.Y., Syu, J.Y., Lin, W.Y. (2013). Source apportionment of $PM_{2.5}$ particle composition and submicrometer size distribution during an Asian dust storm and non-dust storm in Taipei. Aerosol Air Qual. Res. 13, 545–554. https://doi.org/10.4209/aaqr.2012.06.0161

Liu, S.T., Liao, C.Y., Kuo, H.W. (2017). The effects of $PM_{2.5}$ from Asian dust storms on emergency room visits for cardiovascular and respiratory diseases. Int. J. Environ. Res. Public Health. 14, 428–437. https://doi.org/10.3390/ijerph14040428

Liu, X., Pan, X., Wang, Z., He, H., Wang, D., Liu, H., Tian, Y., Xiang, W., Li, J. (2020). Chemical characteristics and potential sources of $PM_{2.5}$ in Shahe city during severe haze pollution episodes in the winter. Aerosol Air Qual. Res. 20, 2741–2753. https://doi.org/10.4209/aaqr.2020.03.0124

Megido, L., Suarez-Pena, B., Negral, L., Castrillon, L., Fernandez-Nava, Y. (2017). Suburban air quality: Human health hazard assessment of potentially toxic elements in PM_{10}. Chemosphere 177, 284–291. https://doi.org/10.1016/j.chemosphere.2017.03.009

Meng, W.J., Shen, H.Z., Yun, X., Chen, Y.L., Zhong, Q.R., Zhang, W.X., Yu, X.J., Xu, H.R., Ren, Y.A., Shen, G.F., Ma, J.M., Liu, J.F., Cheng, H.F., Wang, X.L., Zhu, D.Q., Tao, S. (2020). Differentiated-rate clean heating strategy superior environmental and health benefits in Northern China. Environ. Sci. Technol. 54, 13458–13466. https://doi.org/10.1021/acs.est.0c04019

Pozzer, A., Schultz, M.G., Helmig, D. (2020). Impact of U.S. oil and natural gas emission increases on surface ozone is most pronounced in the central United States. Environ. Sci. Technol. 54, 12423–12433. https://doi.org/10.1021/10.1021/acs.est.9b06983

Si, R., Xin, J., Zhang, W., Wen, T., Li, S., Ma, Y., Wu, X., Cao, Y., Xu, X., Tang, H., Xu, J., Li, X., Wang, Y., Wu, F. (2021). Environmental and health benefits of establishing a coal banning area in the

Beijing-Tianjin-Hebei Region of China. Atmos. Environ. 247, 118191. https://doi.org/10.1016/j.atmosenv.2021.118191

Sternbeck, J., Sjödin, Å., Andréasson, K. (2002). Metal emissions from road traffic and the influence of resuspension — results from two tunnel studies. Atmos. Environ. 36, 4735–4744. https://doi.org/10.1016/S1352-2310(02)00561-7

Su, X.L., Wang, Q., Li, Z.Q., Calvello, M., Esposito, F., Pavese, G., Lin, M.J., Cao, J.J., Zhou, C.Y., Li, D.H., Xu, H. (2017). Regional transport of anthropogenic pollution and dust aerosols in spring to Tianjin – A coastal megacity in China. Sci. Total Environ. 584, 381–392. https://doi.org/10.1016/j.scitotenv.2017.01.016

Tang, M., Liu, Y., He, J., Wang, Z., Wu, Z.J., Ji, D.S. (2021). In situ continuous hourly observations of wintertime nitrate, sulfate and ammonium in a megacity in the North China plain from 2014 to 2019: Temporal variation, chemical formation and regional transport. Chemosphere 262, 127745. https://doi.org/10.1016/j.chemosphere.2020.127745

Tao, J., Gao, J., Zhang, L., Zhang, R., Che, H., Zhang, Z., Lin, Z., Jing, J., Cao, J., Hsu, S.C. (2014a). $PM_{2.5}$ pollution in a megacity of southwest China: source apportionment and implication. Atmos. Chem. Phys. 14, 8679–8699. https://doi.org/10.5194/acp-14-8679-2014

Tao, J., Zhang, L.M., Ho, K.F., Zhang, R.J., Lin, Z.J., Zhang, Z.S., Lin, M., Cao, J.J., Liu, S.X., Wang, G.H. (2014b). Impact of $PM_{2.5}$ chemical compositions on aerosol light scattering in Guangzhou – the largest megacity in South China. Atmos. Res. 135, 48–58. https://doi.org/10.1016/j.atmosres.2013.08.015

Wang, B., Li, N., Deng, F.R., Buglak, N., Park, G., Su, S., Ren, A.G., Shen, G.F., Tao, S., Guo, X.B. (2016). Human bronchial epithelial cell injuries induced by fine particulate matter from sandstorm and non-sandstorm periods: Association with particle constituents. J. Environ. Sci. 47, 201–210. https://doi.org/10.1016/j.jes.2015.12.015

Wang, Q.Q., Huang, X.H.H., Zhang, T., Zhang, Q.Y., Feng, Y.M., Yuan, Z.B., Wu, D., Lau, A.K.H., Yu, J.Z. (2015). Organic tracer-based source analysis of $PM_{2.5}$ organic and elemental carbon: A case study at Dongguan in the Pearl River Delta, China. Atmos. Environ. 118, 164–175. https://doi.org/10.1016/j.atmosenv.2015.07.033

Xu, H., Xiao, Z., Chen, K., Tang, M., Zheng, N.Y., Li, P., Yang, N., Yang, W., Deng, X.W. (2019). Spatial and temporal distribution, chemical characteristics, and sources of ambient particulate matter in the Beijing-Tianjin-Hebei region. Sci. Total Environ. 658, 280–293. https://doi.org/10.1016/j.scitotenv.2018.12.164

Yang, D.Y., Li, Z.Y., Yue, Z.Y., Liu, J.X., Zhai, Z., Li, Z.L., Gao, M.L., Hu, A.L., Zhu, W.J., Ding, N., Li, Z.X., Guo, S.T., Wang, X.X., Wang, L., Wei, J.H (2022). Variations in sources, composition, and exposure risks of $PM_{2.5}$ in both pre-heating and heating seasons. Aerosol Air Qual. Res. 22, 210333. https://doi.org/10.4209/aaqr.210333

Yao, L., Yang, L.X., Yuan, Q., Yan, C., Dong, C., Meng, C.P., Sui, X., Yang, F., Lu, Y.L., Wang, W.X. (2016). Sources apportionment of $PM_{2.5}$ in a background site in the North China Plain. Sci. Total Environ. 541, 590–598. https://doi.org/10.1016/j.scitotenv.2015.09.123

Zhai, S.X., Jacob, D.J., Wang, X., Shen, L., Li, K., Zhang, Y.Z., Gui, K., Zhao, T.L., Liao, H. (2019). Fine particulate matter ($PM_{2.5}$) trends in China, 2013-2018: Separating contributions from anthropogenic emissions and meteorology. Atmos. Chem. Phys. 19, 11031–11041. https://doi.org/10.5194/acp-19-11031-2019

Zhang, F.W., Xu, L.L., Chen, J.S., Chen, X.Q., Niu, Z.C., Lei, T., Li, C.M., Zhao, J.P. (2013a). Chemical characteristics of $PM_{2.5}$ during haze episodes in the urban of Fuzhou, China. Particuology 11, 264–272. https://doi.org/10.1016/j.partic.2012.07.001

Zhang, R., Jing, J., Tao, J., Hsu, S.C., Wang, G., Cao, J., Lee, C.S.L., Zhu, L., Chen, Z., Zhao, Y., Shen, Z. (2013b). Chemical characterization and source apportionment of $PM_{2.5}$ in Beijing: Seasonal perspective. Atmos. Chem. Phys. 13, 7053–7074. https://doi.org/10.5194/acp-13-7053-2013

Zhu, Y.H., Huang, L., Li, J.Y., Ying, Q., Zhang, H.L., Liu, X.G., Liao, H., Li, N., Liu, Z.X., Mao, Y.H., Fang, H., Hu, J.L. (2018). Sources of particulate matter in China: Insights from source apportionment studies published in 1987–2017. Environ. Int. 115: 343–357. https://doi.org/10.1016/j.envint.2018.03.037